Whitepaper

Electrochemical Impedance Spectroscopy Moves out of the Lab and into the Field for Next-Generation of Battery Systems

Gert Renkema, Design Engineer, BMS Systems
Philippe Perruchoud, Applications Manager, BMS Systems
Martin Royer, Hardware Manager, BMS Systems
Dr. Wenzel Prochazka, Senior Product Manager, BMS Systems

Introduction

Electrochemical Impedance Spectroscopy (EIS) is a powerful technique for probing the internal states and dynamics of lithium-ion cells' electrodes. It provides insights into electrochemical processes and cell-level local differences of these processes by analyzing the cell's response to small AC perturbations across a several of frequencies. It has emerged as a cornerstone technique in the characterization and diagnostics of lithium-ion cells in manufacturing. As the demand for high-performance, safe, and long-lasting energy storage systems intensifies, driven by applications in electric vehicles, consumer electronics, and grid storage, EIS offers a nondestructive, highly informative method to add robust control mechanisms to battery management systems.

In this whitepaper, we present a comprehensive overview of EIS as applied to lithium-ion cells, integrating insights from experimental studies, physics-based modeling, and advanced diagnostic applications. We also explore how EIS reveals key battery cell electrode-level behaviors, including charge transfer resistance, solid-state diffusion, and electrolyte conductivity, and how these parameters evolve with temperature and state of health (SoH) and state of function (SoF), both included in the state of X vector (SoX).

Recent advancements, such as dynamic EIS (DEIS), enable real-time monitoring of phenomena like lithium plating, which is an adverse effect that compromises battery safety and longevity. DEIS allows impedance measurements during battery charging, offering a pathway to safer fast-charging protocols and robust in-field monitoring of batteries, due to consistent preconditioning before EIS measurement. Additionally, EIS-based methods have proven effective in estimating internal cell temperature and detecting early-stage internal short circuits, enhancing battery management system (BMS) capabilities. [11]

Beyond performance diagnostics, EIS also plays a role in safety assurance. Manufacturing defects, such as burrs on electrode tabs, have been linked to catastrophic failures. Studies using computed tomography and impedance analysis highlight the importance of integrating EIS with quality control to prevent thermal runaway [6 & 13]. By synthesizing technical findings from multiple sources, this paper aims to guide engineers, researchers, and product developers in leveraging EIS for improved battery design, monitoring, and safety.

The following sections delve into the principles, measurement techniques, modeling approaches, and practical applications of EIS in the context of lithium-ion cell technology.

Fundamentals of EIS in lithium-ion cells

In this chapter, we introduce the core concepts of EIS through three key lenses: Nyquist and Bode plots, equivalent circuit models (ECMs), and interpretation of impedance features.

1. Nyquist and Bode plots

The Nyquist plot (Figure 1) is a graphical representation of impedance where the real part (Re(Z)) is plotted on the x-axis and the negative imaginary part (-Im(Z)) on the y-axis. It typically reveals semicircular arcs and linear tails, each corresponding to different electrochemical processes.

A. High-frequency tail indicates electric fields in the electrode stack and conductors

B. Middle-frequency arcs represent charge transfer resistance

C. Low-frequency tail indicates solid diffusion limitations by its angle.

D. The ohmic offset from real zero represents the resistance losses due to the electrode geometry and the wires used for measurement

The Bode plot complements the Nyquist plot by showing the magnitude of impedance |Z| and phase angle as functions of frequency. It is particularly useful for identifying time constants and evaluating system stability.

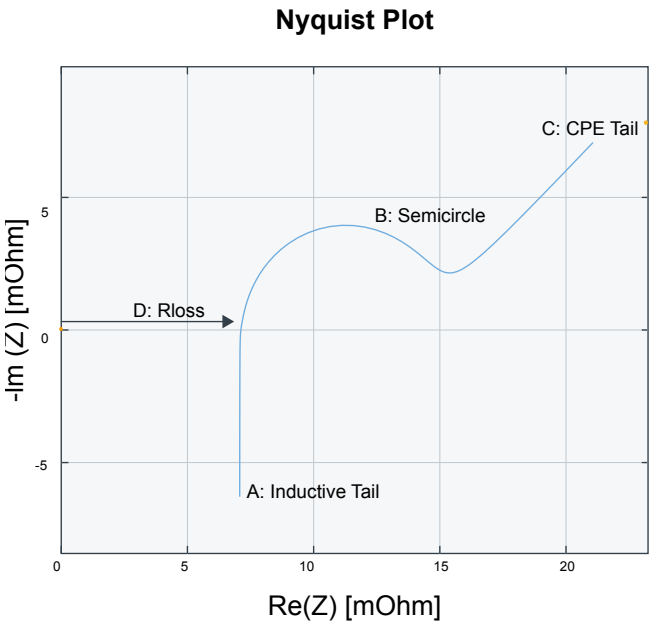

Figure 1: Simulated Nyquist plot.

2. Equivalent circuit models (ECMs)

To interpret EIS data, researchers often use ECMs that mimic the battery's behavior using electrical components. A typical ECM includes parts that represent the elements found in the Nyquist graph:

- **L1:** Inductance to represent A
- **Rs:** Series resistance representing D
- **Rkin & Ckin:** RC element representing B
- **CPE:** Constant Phase Element, representing C

Using such a model, the voltage behavior of a cell can be modelled from its current, temperature, and state-of-charge (SoC) inputs. This is why such models are often used in model-based BMS SoX estimation algorithms for the SoC [3]. Using EIS can support the parameter finding during development of such models, as well as the parameter adaptation over State-of-Health (SoH) in the application. [1]

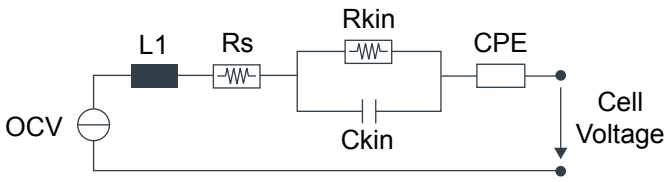

Figure 2: ECM example.

3. Interpreting impedance features in lithium-ion cells

The impedance spectrum of a lithium-ion cell encodes rich information about its internal electrochemical processes and states. In a Nyquist plot, the high-frequency intercept on the real axis corresponds to the ohmic resistance (Rs), encompassing contributions from the electrolyte, current collectors, and contacts (tabs, wiring, etc.). The mid-frequency semicircle reflects the charge transfer resistance from the solid material to the liquid, which is overlayed for both electrodes, creating the known semi-ellipse shape and well seen at low temperatures [2] (Rkin) and double-layer capacitance at both electrodes to the electrolyte interface. At low frequencies, the so-called "Warburg tail" indicates diffusion limitations in the solid phase, which is shaped based on particle size distribution and solid intercalation capacity [14].

High-frequency intercept: Series resistance (Rs)

Semicircle diameter: Charge transfer resistance (Rkin)

Low-frequency slope: Warburg impedance, indicating ion diffusion

Recent studies, such as [4], demonstrate that DEIS can reveal subtle changes in these features during charging. For instance, the onset of lithium plating manifests as a reduction in the semicircle diameter, particularly in the midfrequency region, due to a parallel current path bypassing the interfacial impedance. This phenomenon is detectable by monitoring the difference between the minimum of Rs and the average Rs of cells, or by observing shifts in the imaginary part of the impedance (minimum to maximum value of imaginary part of the top of the semicircle), which are less sensitive to temperature and SoC variations.

While others report a tilting counterclockwise of the semicircle as a result of short circuits [6 & 13].

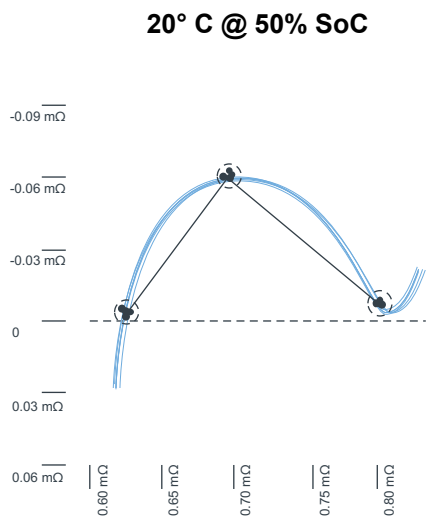

Figure 3: Interpretation of semicircle B with three characteristic frequencies, comparing the standard deviations of multiple cell measurements (own graphics).

Both of these effects are not well detectable with standard time-based BMS controls, since their behaviour changes are faster in time (e.g., spikes indicating short circuits) than the usual time interval for data acquisition (20-100ms). While with EIS the semicircle behaviour can be sufficiently described by using three characteristic frequencies as shown in Figure 3

Such interpretations enable engineers of BMS systems to do real-time diagnostics of plating, aging, and thermal effects, not only in a Lab setup, but also directly in-field in a battery system made of many cells in series or parallel. This makes it possible to enhance battery safety and performance, and detect early signs of failure.

Measurement techniques and practical considerations

1. Galvanostatic vs. potentiostatic EIS

EIS can be performed in two modes: galvanostatic (GEIS) and potentiostatic (PEIS). In GEIS, a small AC current is applied and the resulting voltage response is measured. This mode is preferred for lithium-ion cells due to their low impedance, which ensures better control of the excitation response not overshooting and accuracy of measurement. In contrast, PEIS applies a small AC voltage and measures the resulting current. PEIS is more suitable for high-impedance systems, as GEIS would trigger large voltage signals easily. Therefore, the choice between GEIS and PEIS depends on the cell characteristics and the measurement goals. In low-impedance lithium-ion cells, GEIS provides more reliable data, especially in the mid-frequency range where charge transfer processes dominate.

2. Frequency ranges and excitation levels

The frequency range in EIS typically spans from multiple kHz to mHz. With the 1kHz measurement being a long-standing industry standard in short circuit detection in manufacturing and 1-10Hz as the usual control frequency of classic BMS. Higher frequencies probe inductive and ohmic behaviors, while low frequencies reveal diffusion and capacitive effects. However, measuring at very low frequencies (<0.1Hz) requires long acquisition times, increasing the risk of drift and noise. A typical laboratory R&D measurement is a "frequency sweep", which starts at high frequency and proceeds downward logarithmically. A typical application-related measurement will pick out certain single frequencies and use the single (or two, three frequencies combined) behaviour as controls parameter.

Excitation levels must be carefully chosen to balance linearity, thermal effects, and signal-to-noise ratio (SNR) for the unit under examination and its environment. A common practice is to use an AC current of C/20, which minimizes non-linear effects and avoids self-heating, but which might render the response signal insufficient, especially in high power cells (e.g., 48V hybrid powertrain applications). The excitation waveform is historically a pure sine wave, initiated at a zero crossing to prevent transients and make the mathematical Fourier transformation easy. In modern devices, any kind of cyclical waveform (square w/wo bias or triangular) may be used. It must be mentioned, though, that the test results of different excitation types must not be compared to each other [12]. Measurement accuracy is influenced by the excitation amplitude and duration, with longer durations improving low-frequency resolution.

3. Temperature and SoC dependences

Temperature and SoC significantly affect the impedance characteristics of lithium-ion cells. At lower temperatures, internal resistance increases, leading to larger semicircles in Nyquist plots. As the temperature rises, the semicircle diminishes due to enhanced charge transfer kinetics. SoC influences are more subtle, typically affecting the impedance at extreme values (close to 0% and 100%). The larger response amplitude of Temperature changes and basic flatness in the mid SoC range is also the reason why pure SoC estimation with EIS is challenging, if possible at all.

To characterize these dependencies, a multidimensional dataset is required, mapping impedance across temperature, SoC, and frequency. A typically recommended protocol involves charging the cell to a target SoC at room temperature, then cycling through temperature steps while measuring EIS at equilibrium. This ensures consistent SoC and avoids specification violations. But it does not really provide a constant preconditioning and it is most probably not suitable for in-application measurements to be comparable to parameterization. Reducing the number of SoC steps can accelerate the process, as most variations occur at the extremes. Also, doing the parameterization measurement with a constant charge current overlay ensures typically reachable preconditioning in applications, but measurement design of the experiment and computation of bias-free values becomes more complicated.

Applications of EIS in lithium-ion battery diagnostics

1. State of health (SoH) estimation

As batteries are used, they age, which means that their internal resistance increases due to degradation mechanisms such as SEI layer growth and electrolyte decomposition, while the capacity available to discharge reduces due to mechanisms such as loss of active material. EIS can detect these changes by analyzing the Nyquist plot, where the diameter of the semicircle correlates with charge transfer resistance. By comparing impedance responses over time, state of health (SoH) algorithms can be supported in their accuracy of quantifying and separating resistance increase from capacity decrease. For example, a shift in the mid-frequency arc or an increase in the real part of impedance at low frequencies can indicate capacity fade. This method is non-invasive and can be implemented in BMS for real-time monitoring [12]. There are more details in this paper in a later chapter.

2. Temperature estimation via zif and cost function methods

Temperature estimation is critical for safe and efficient battery operation. EIS enables sensorless core temperature estimation using methods such as zero intercept frequency (ZIF) and cost function minimization [8]. The ZIF method identifies the frequency at which the imaginary part of impedance crosses zero, which correlates with internal temperature. This frequency decreases with increasing temperature and is relatively independent of SoC. Alternatively, the cost function method compares measured impedance at selected frequencies with a pre-characterized dataset to find the best temperature match. Both methods have been validated experimentally and show high accuracy within the normal operating range. While it is very important to note that the results of the studies always are very much dependent on the immediate history of current loading onto the cell in order to achieve good correlation. Either an active preconditioning (e.g., charge with defined current for 15min) or a long rest period (>3h) are needed.

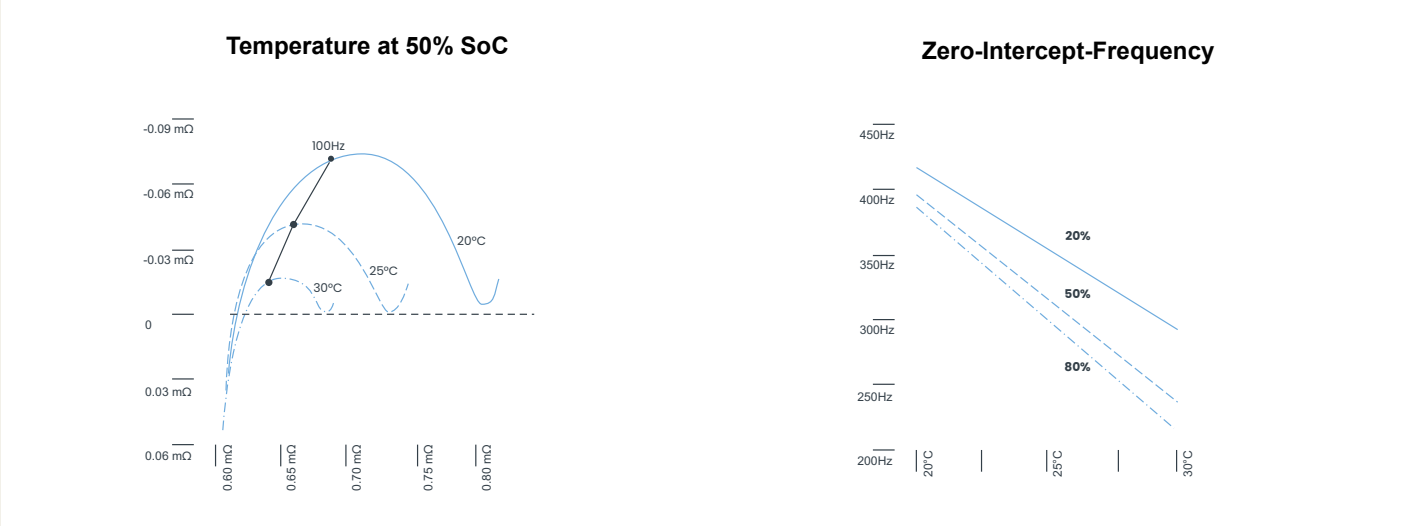

Figure 4: ZIF vs. temperature and SOC for an NMC cell measured by NXP.

3. Detection of internal short circuits

Internal short circuits (ISC) pose serious safety risks in lithium-ion batteries. EIS provides a sensitive method for early ISC detection by analyzing changes in low-frequency impedance. Studies show that ISC primarily affects the diffusion-controlled region, reducing the phase angle and altering the impedance tail [6]. For example, a decrease in the imaginary part of impedance at low frequencies or a shift in the Nyquist plot slope can indicate ISC onset. Experimental validation using coin cells with induced ISC and commercial cells with substituted ISC resistances demonstrates that EIS can detect ISC even at early stages. Figures from the literature show how the impedance spectrum changes with ISC severity and aging, highlighting EIS as a diagnostic tool.

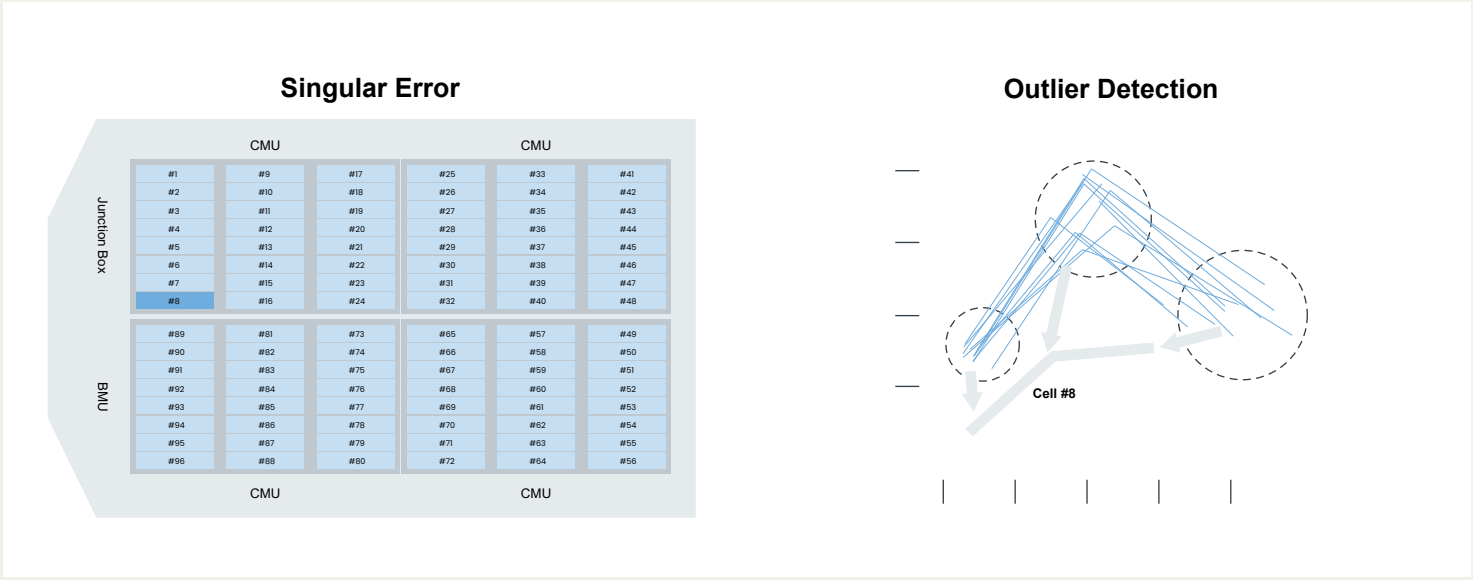

Figure 5: EIS performance comparisons between the cell with ISC and normal cells.

Model-based interpretation of EIS

As shown above, EIS provides a rich dataset for understanding the internal processes and states of lithium-ion cells. However, interpreting this data requires robust modeling approaches that can link impedance features to physical phenomena, the geometry of the cell, and the measurement setup.

This chapter explores three key aspects of model-based interpretation: physics-based models, parameter fitting challenges, and the influence of cell geometry on impedance.

1. Physics-based models as an upgrade to ECM baseline

Physics-based models aim to represent the actual electrochemical and transport processes occurring within the battery. These models often build on porous electrode theory, incorporating elements such as charge transfer resistance, double-layer capacitance, and solid-state diffusion. Unlike ECMs, which use lumped components to fit impedance spectra, physics-based models derive parameters from physics principles and experimental data. For example, the transmission line model (TLM) is commonly used to describe porous electrodes, capturing the distributed nature of ionic and electronic conduction [7]. These models are particularly valuable for diagnosing aging mechanisms, such as SEI growth or loss of active material, by linking changes in impedance to specific degradation pathways.

2. Parameter fitting and uniqueness challenges

Fitting impedance data to models, whether ECMs or physics-based, poses significant challenges. One major issue is parameter uniqueness: multiple parameter sets can yield similar fits, making it difficult to identify the true physical values. This is especially problematic in ECMs with many degrees of freedom. To mitigate, researchers use constraints based on known material properties or complementary measurements (e.g., three-electrode setups). Additionally, fitting algorithms must balance accuracy with computational efficiency. Techniques such as Kramers-Kronig validation and distribution of relaxation times (DRT) analysis help ensure that fitted models are physically meaningful and robust across operating conditions. Such DRT parameters can be read from EIS data.

3. Impedance contributions of different cell geometries

Cell geometry plays a critical role in shaping the impedance response, particularly at high frequencies. Studies [5 & 9] demonstrate that cylindrical cells exhibit complex resistive-inductive behavior due to their spiral-wound architecture. Using planar transmission line models and vector network analyzer (VNA) measurements, these works show how tab placement, winding number, and electrode thickness influence impedance.

For instance, Schindler's model reconstructs the impedance of a commercial 18650 cell by combining electrochemical data from extracted electrodes with geometrical parameters from microscopy. The model reveals that tab positions affect current density distribution, altering both resistive and inductive losses. Landinger's study extends this by analyzing impedance at usual kHz EIS levels, showing that high-power cells with more windings exhibit greater inductance, while tab alignment (parallel vs. antiparallel) modulates mutual inductive coupling.

Similarly, other studies show the EIS dependence on pouch or prismatic cell stacks, even compared to their own stamp outs [10].

These insights underscore the importance of geometry-aware modeling in EIS interpretation, especially for applications involving high-frequency signals or power electronics integration.

Aging effects and EIS sensitivity

As cells degrade over time due to cycling, temperature, and calendar aging, their impedance spectra evolve in ways that reflect underlying physical and chemical changes. In this chapter, we explore three key aging-related phenomena detectable via EIS: SEI growth and charge transfer resistance, diffusion impedance and electrode degradation, and high-frequency inductive changes due to structural aging.

1. SEI growth and charge transfer resistance

One of the earliest and most prominent aging effects in lithium-ion cells is the growth of the Solid Electrolyte Interphase (SEI) layer on the anode. This passivation layer increases the charge transfer resistance (Rkin), which manifests as an enlarged semicircle in the midfrequency region of the Nyquist plot. Over time, the SEI becomes thicker and more resistive, leading to a measurable increase in Rkin. Studies using three-electrode setups have confirmed that the anode contributes significantly to this impedance growth. Additionally, the SEI can trap lithium ions, reducing available capacity and increasing polarization. EIS allows for non-invasive tracking of these changes, making it a valuable tool for estimating SoH. Please be aware that for tracking these changes over time in an in-application measurement setup, the preconditioning for the repeatability and comparability plays a paramount role.

2. Diffusion impedance and electrode degradation

Aging also affects the diffusion of lithium ions within the electrode materials. As active material becomes isolated due to particle cracking or loss of electrical contact, the Warburg impedance—visible as a slope in the low-frequency region—changes in magnitude and shape according to the changes in solid diffusion. Increased tortuosity and reduced porosity in aged electrodes slow down ion transport in the liquid phase, leading to a steeper and more extended Warburg tail [7]. This is particularly evident in high-energy cells with thick electrodes, where degradation leads to uneven current distribution and localized overpotentials. EIS can quantify these changes by fitting the low-frequency region to transmission line models or porous electrode theory.

3. High-frequency inductive changes due to structural aging

At high frequencies, structural changes in the cell—such as tab corrosion, current collector delamination, or winding deformation—can alter the inductive characteristics of cylindrical cells. Studies by [9 & 5] show that the inductive behavior of the jelly roll is sensitive to tab placement and winding integrity. As cells age, mechanical stresses can shift tab positions or reduce mutual inductive coupling between layers, leading to changes in the high-frequency impedance arc. These effects are visible in the fourth quadrant of the Nyquist plot and can be modeled using transmission line approaches that incorporate both electrochemical and electrical domains.

Dynamic EIS and in-situ monitoring

EIS has traditionally been used in controlled laboratory settings to characterize lithium-ion cells. However, recent advancements in DEIS have enabled real-time impedance measurements during battery operation, opening new possibilities for in-situ diagnostics and integration with BMS.

1. Real-time EIS during operation

Dynamic EIS involves superimposing a small AC signal onto the DC current during charging or discharging, allowing impedance spectra to be captured without interrupting the battery's operation. As shown in studies by [4], DEIS can identify the onset of plating by monitoring changes in the mid-frequency semicircle of the Nyquist plot, where charge transfer resistance decreases due to parallel plating currents.

The key to successful DEIS is maintaining quasi-stationary conditions during measurement. This requires careful selection of excitation frequency and amplitude to avoid violating linearity and causality. Typically, frequencies between mHz and up to multiple kHz are used, with AC amplitudes adjusted to maintain voltage perturbations below 10 mV. Validation using Kramers-Kronig tests ensures the reliability of the impedance data.

2. Implications for battery management systems

Integrating DEIS into BMS architecture transforms battery monitoring from passive voltage and current tracking to active electrochemical diagnostics. Real-time impedance data then ties to the BMS estimation algorithms for cell internal temperature calculation from outside sensors and detection of early signs of degradation.

Moreover, DEIS allows for continuous monitoring of impedance features that correlate with SoH. These insights can be used to adapt charging protocols dynamically, preventing conditions that accelerate degradation or trigger safety risks.

The challenge lies in embedding DEIS hardware and algorithms into compact, low-power BMS units. Recent developments in embedded impedance analyzers being integrated in automotive-type integrated circuits and signal processing techniques integrating direct Fourier transformer (DFT) hardware have made it feasible to introduce a complete working chipset for automotive conditions. (i.e. NXP's EIS-enabled battery management chipset – www.nxp.com/BMS-EIS) This is paving the way for smart batteries capable of self-diagnosis and adaptive control.

NXP is providing a BMS chipset with EIS-enabled devices, which have the same printed circuit board (PCB) footprint and pinning of the package as the non-EIS devices. The EIS-enabled Chipset consists of the BMA6402 Gateway and synchronization master, the BMA7418 battery cell controller and per cell voltage DFT, as well as the BMA8420 battery junction box controller and current DFT. Also, for the excitation, an NXP device doubling as a pre-charge controller as well, the TAA3033, completes the system.

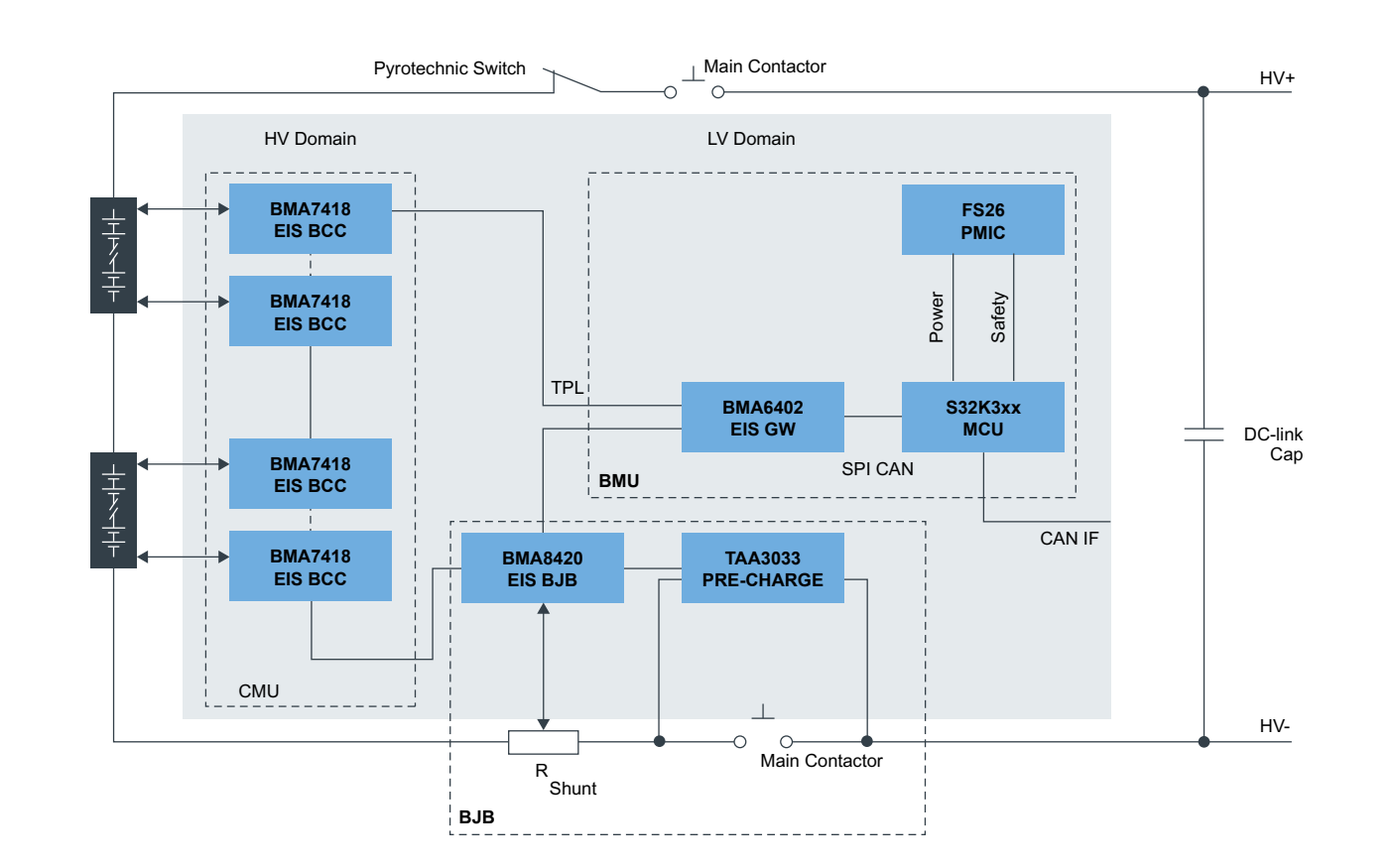

Figure 6: Block diagram of NXP EIS enabled devices.

3. Wire harness influences on EIS

In practical applications, the accuracy of EIS measurements can be significantly affected by the wire harness and associated cabling used to connect cells to measurement equipment or embedded systems.

These parasitic elements introduce phase delays and impedance artifacts that can mask or mimic internal cell features.

For example, the inductance of a wire harness can add a steep imaginary component to the Nyquist plot, falsely suggesting increased internal inductance. To mitigate this, impedance measurements must be de-embedded from the harness using reference standards or calibration techniques, such as measuring a dummy cell with known impedance.

In embedded BMS environments, careful PCB layout, shielding, and connector design are essential to preserve signal integrity. Additionally, modeling approaches must include harness-induced impedance elements to accurately simulate system-level behavior. As dynamic EIS becomes more integrated into real-time monitoring, understanding and compensating for wire harness effects is critical for reliable diagnostics and control.

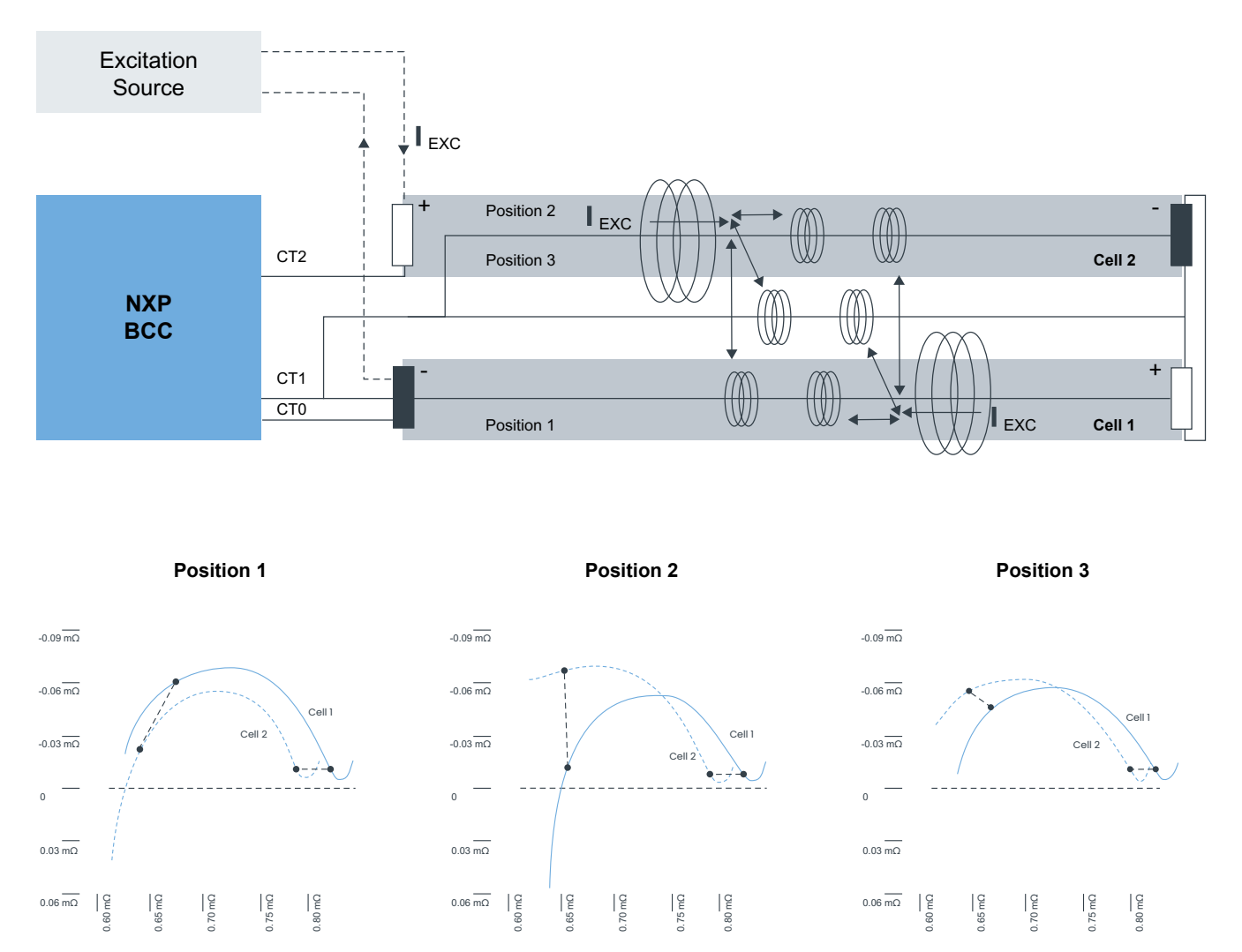

Figure 7: Wire harness positioning influence in Nyquist curve (own picture). The three positions indicate different geometrical routing of the measurement wire in relation to the physical flow of load current.

EIS equipment and accuracy considerations

Precise synchronization is the foundation of reliable EIS in parallel multi-measurement setups (either multiple cells or multiple cells with multiple excitation currents). Phase accuracy determines how faithfully impedance spectra reflect real electrochemical behavior across a battery pack, and even small timing errors can distort results or mask critical insights into battery health. The level of precision is critical for interpreting subtle impedance shifts that indicate internal short circuits, aging, or degradation, giving engineers confidence that their diagnostics are both accurate and actionable. This chapter explores two key aspects: instrumentation requirements and error models with SNR considerations.

1. Synchronization

Accurate EIS measurements require precise synchronization between the excitation signal, cell voltage acquisition, and current measurement. This becomes particularly challenging in centralized Battery Management System (BMS) architectures, where multiple Battery Cell Controller (BCC) ICs—each operating on independent clocks—measure cell voltages, while current is typically measured only once at the battery stack level. Additionally, the excitation signal may be generated by a separate subsystem, such as a DC/DC converter or inverter, further complicating synchronization. When these subsystems operate on different clock domains, several critical synchronization challenges arise:

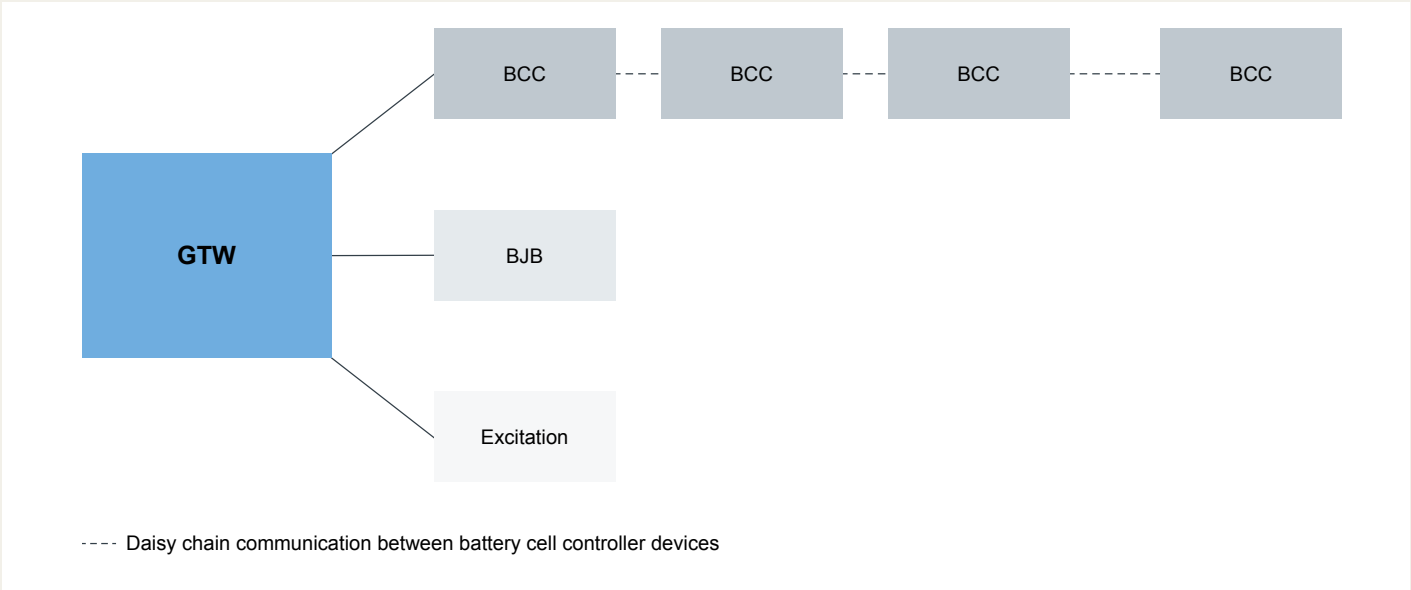

Figure 8: Gateway hardware-based synchronization of the devices in the BMS chipset.

Excitation synchronization. The excitation signal must be tightly aligned with the frequency used in the Discrete Fourier Transform (DFT) analysis. If the excitation frequency is not synchronized with the measurement system, amplitude and phase errors are introduced, resulting in inaccurate impedance values. This misalignment prevents the measured response from accurately reflecting the cell's behavior at the intended frequency.

To ensure measurement accuracy, it is recommended to verify the excitation frequency for each impedance measurement or sweep. The NXP EIS chipset includes a mechanism that measures and corrects alignment between the excitation signal and the DFT frequency, thereby minimizing phase and amplitude errors.

Start of EIS synchronization. Synchronization of the start of the EIS measurement is equally critical. The DFT analysis must begin simultaneously across all Analog Front End (AFE) ICs involved in voltage and current acquisition. If the start times are not aligned, phase discrepancies occur, which become increasingly significant at higher excitation frequencies. This issue is particularly relevant in systems where BCCs are daisy-chained for communication, as propagation delays can lead to asynchronous sampling. A robust synchronization mechanism is required to ensure all devices initiate sampling at the same time.

Analog front end (AFE) clock synchronization. Each BCC's AFE typically operates on its own local clock, which can drift over time and with temperature variations. Unsynchronized AFE clocks result in sampling jitter and drift, leading to cumulative amplitude and phase inaccuracies throughout the EIS sweep.

These errors degrade the fidelity of impedance measurements and can obscure the estimation of the cell's critical electrochemical characteristics.

The NXP EIS chipset addresses this challenge by providing accurate synchronization of AFE clocks within the daisy chain. This enables coordinated sampling of cell voltages in the pack and current with a standard deviation of less than 150 ns over the entire impedance measurement duration, ensuring high-resolution and reliable data.

2. Error models

Measurement accuracy in EIS is influenced by both systematic and random errors.

Systematic errors arise from parasitic inductance, contact resistance, and calibration drift, while random errors are primarily due to noise in the measurement signal. The SNR becomes especially critical at high frequencies, where impedance magnitudes are low and the imaginary component dominates.

To mitigate these issues, reference measurements using dummy cells (e.g., solid copper cylinders) are employed to de-embed the cell impedance from the test setup.

Systematic errors introduced by the setup contribute directly to the absolute error of the impedance result. One common source of systematic error is gain error in the cell voltage measurement path. Unlike offset errors, which are irrelevant in impedance analysis due to its focus on AC signals, gain errors affect the amplitude accuracy of the measured voltage response. For example, in the NXP EIS chipset, the voltage measurement accuracy is specified at ±1.2 mV for a nominal cell voltage of 3.7 V. If the

excitation current induces a cell voltage amplitude of 1 mV, the gain error translates to an impedance measurement error of just 0.03%.

Error modeling also involves understanding the frequency-dependent behavior of the measurement system. This includes all filtering in the signal path, for example, analog anti-aliasing filters and digital decimation (down-sampling) filters. Also, timing errors could degrade performance at higher frequencies, especially the phase angle of the impedance.

Achieving high accuracy in EIS requires not only advanced instrumentation and wiring but also rigorous error modeling, correction and validation protocols. These considerations are essential for reliable diagnostics, especially in applications involving dynamic loads or high-frequency signal environments

3. A simple noise-based error model

A straightforward noise-based error model links the relative error in voltage magnitude |V| to the phase error in arg(V), expressed in radians:

- Relative error in |V| ≈ Phase error in arg(V)
  - Example: A 1% error in |V| corresponds to a phase error of approximately 0.01 radians (≈ 0.57°).
  - Mathematically: PE ≈ arctan(|r|/|V|) ≈ |r|/|V| for small |r|.

The result from above, RME = PE, does not contain any information about (or restriction to) a particular frequency: it holds for any frequency.

For example, if noise is white noise (flat spectrum over frequency) then the EIS system performance will not depend on frequency as long as this noise is the dominant source of errors. If the noise is not white, then the frequency dependence of the errors will follow the frequency dependence of the noise.

EIS system performance will depend on the duration of the measurement (in seconds, not the number of signal periods!). So, we can achieve frequency-independent performance only when:

- Noise is white noise
- Duration of any measurement is constant

However, a constant duration of d seconds limits the lowest usable frequency to 1/d Hz.

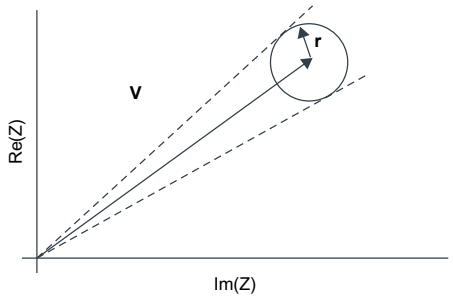

Figure 9: Simple error model (NXP own graphics)

EIS current excitation

EIS for batteries in applications is performed by repetitively sourcing and sinking current from and into the battery from a secondary energy storage in the system (e.g., capacitors or other batteries) and measuring back the voltage ripple. Current automotive battery cells have a very low impedance (below 1mOhm), and the excitation current must generate sufficient voltage ripple for measuring back a level with a good signal-to-noise ratio. Typical amplitudes for excitation currents range from 2 A to 10 A to limit self-heating, with a typical level of 5A.

Multiple waveforms are feasible with the fundamental frequency and the intended amplitude. This includes Sine wave, square wave or triangles. The excitation current can be superimposed on a DC charge current or load current or can flow through the battery that is in an idle state without charge or load current.

Methods

There are several methods to generate this excitation current. The most basic method is loading the 800 V battery in a resistive way, but then the energy will be dissipated and lost. As it is undesirable to waste energy, an important objective is to generate the excitation current in an efficient way without losing energy and without degrading the autonomy of the electrical vehicle.

Other methods are using the onboard charger or the DCDC converter in order to modulate the load current on the high voltage side.

One method uses the DC-link capacitor as a reservoir for storing and sourcing the energy for EIS. A second method involves splitting the battery pack and sourcing current from one half-pack, then sinking it into the other half-pack, and vice versa.

EIS with DC-link capacitor

The advantage of using the DC-link capacitor is that it provides an EIS solution solely within the BMS system. This method can be applied in parking mode and charging mode, but not in driving mode because the main contactors are open.

During EIS, the contactors K1 and K2 are non-conducting, and contactors K3 and K4 are conducting, allowing a variable DC-link voltage between 0V and the 800V battery voltage. The EIS excitation frequency is determined by the NXP BMA8420 controller and applied to the gate drivers GD1 and GD2 of the half-bridge. The half-bridge defines the current direction; if switch Q1 is conducting, then the excitation current flows from the battery to the DC-link capacitor with buck conversion, and if switch Q2 is conducting, the current flows back from the DC-link capacitor towards the battery via boost conversion.

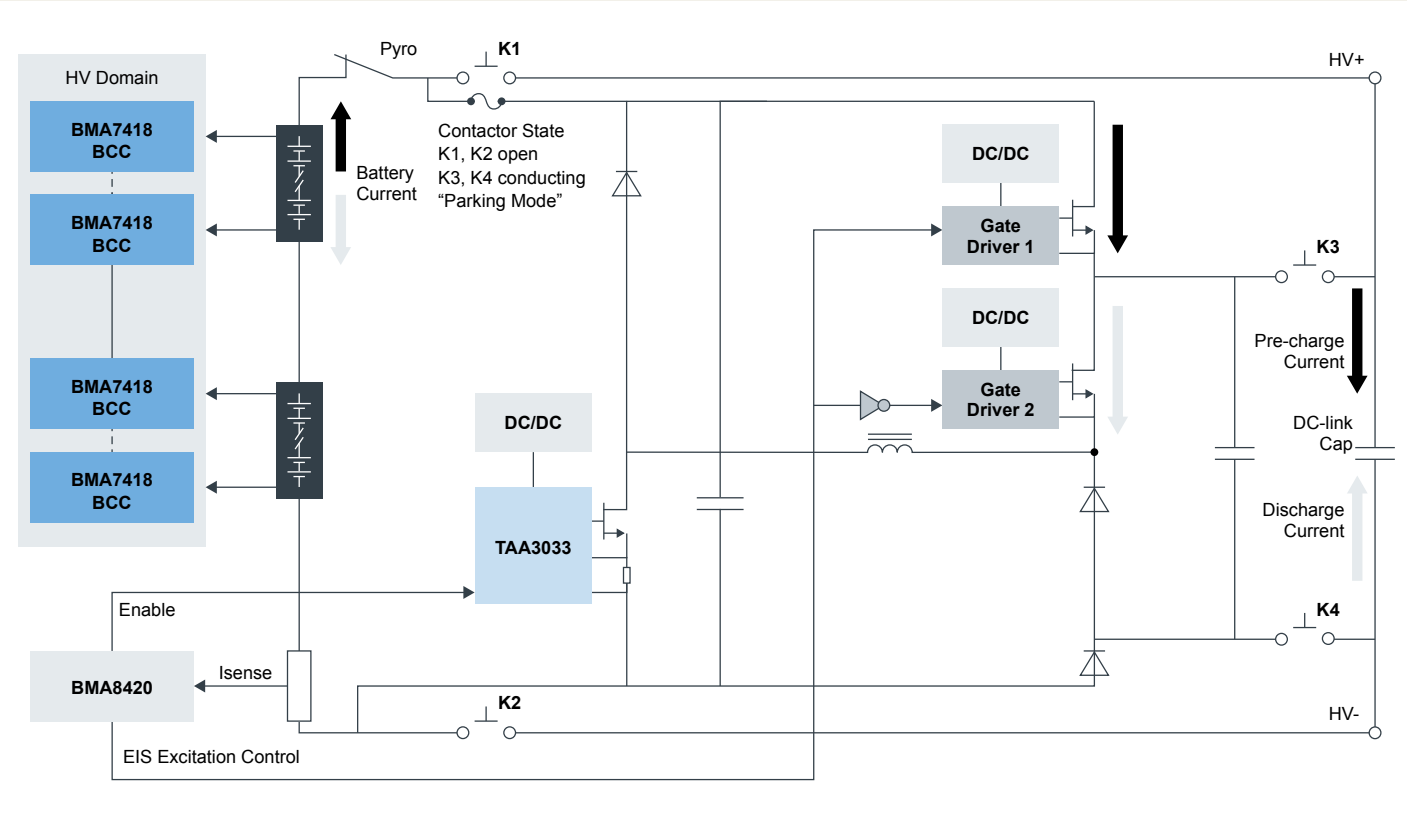

Figure 11: Pre-charge based excitation (NXP own diagram).

EIS with battery half-pack

The battery pack is normally divided into two or more parts, and this allows the EIS operation between two battery half-packs of 400V each. One battery half-pack sources the excitation current, and the other half-pack sinks the excitation current. The generation of the excitation current is by buck-boost conversion, and because both half-packs have equal voltage, the source and sink excitation currents are also equal.

One of the two TAA3033 controllers is active at the time. The active controller discharges the parallel half-pack in the primary stroke of the buck-boost conversion, and this energy is stored in the inductor. At the turning off of the power switch, the inductive energy is transmitted to the other half-pack with a recirculation current that flows via the body-diode of the other power switch that is connected to the non-active controller. The capacitors are added for filtering the battery half-pack currents.

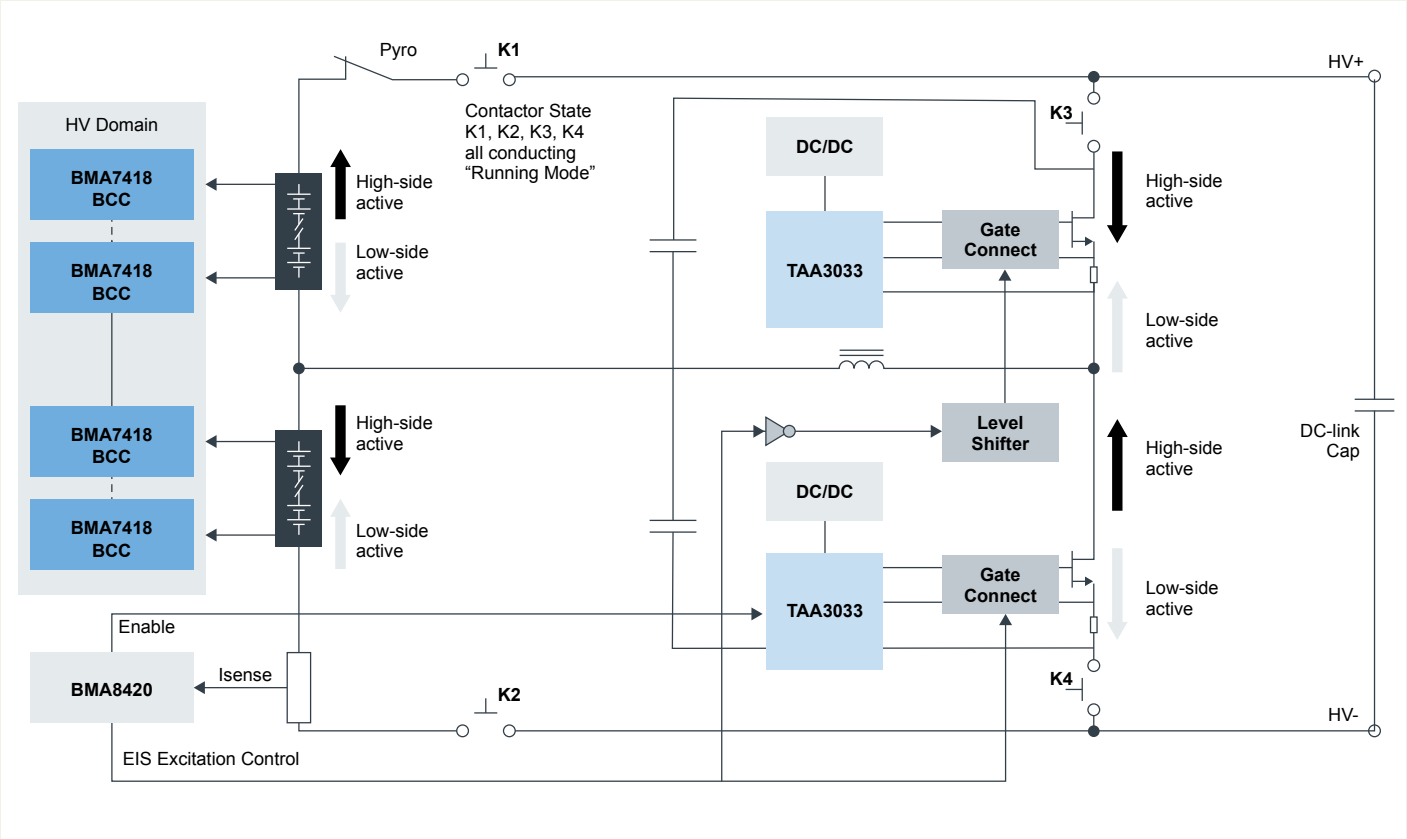

Figure 12: Pre-charge based excitation (NXP own diagram).

Conclusion

EIS is poised to become a cornerstone diagnostic tool in the future of automotive and ESS battery packs. As battery systems grow in complexity and scale, the ability to non-invasively monitor internal states such as temperature, SoH, and degradation mechanisms becomes increasingly valuable. EIS offers a unique window into these internal processes, enabling predictive maintenance, enhanced safety, and optimized performance.

In automotive applications, the integration of real-time EIS into BMS will support advanced functionalities such as dynamic thermal management, early fault detection, and adaptive fast charging strategies.

For ESS deployments, EIS can improve uptime and lifecycle economics by identifying cell imbalances and aging trends across large-scale arrays.

Looking ahead, the miniaturization of EIS hardware, improvements in signal processing, and robust modeling frameworks will be key enablers for widespread adoption. As standardization and computational integration progress, EIS will transition from a laboratory tool to an embedded, real-time feature in next-generation battery systems, supporting the electrification of transport and the global shift toward renewable energy and enabling a predictive thermal runaway prevention strategy.

References

1. Ak, J., Burak, C., Ugur, Y., Nessa, F., Mingzhao, Z., Ferran, B., & Widanage, W. (2024). Development and validation of physics-based model for lithium-ion battery degradation across various aging conditions: Electrochemical model parameterisation and validation. ResearchGate. https://doi.org/10.13140/RG.2.2.16600.92165

2. Andre, D., Meiler, M., Steiner, K., Wimmer, C., Soczka-Guth, T., & Sauer, D. U. (2011). Characterization of high-power lithium-ion batteries by electrochemical impedance spectroscopy. I. Experimental investigation. Journal of Power Sources, 196(12), 5334–5341. https://doi.org/10.1016/j.jpowsour.2010.12.102

3. Hametner, C., Jakubek, S., & Prochazka, W. (2018). Data-driven design of a cascaded observer for battery state of health estimation. IEEE Transactions on Industry Applications, 54(6), 6258–6266. https://doi.org/10.1109/TIA.2018.2851231

4. Koseoglou, M., Tsioumas, E., Ferentinou, D., Jabbour, N., Papagiannis, D., & Mademlis, C. (2021). Lithium plating detection using dynamic electrochemical impedance spectroscopy in lithium-ion batteries. Journal of Power Sources, 512, 230508. https://doi.org/10.1016/j.jpowsour.2021.230508

5. Landinger, T. F., Schwarzberger, G., & Jossen, A. (2021). High frequency impedance characteristics of cylindrical lithium-ion cells: Physical-based modeling of cell state and cell design dependencies. Journal of Power Sources, 488, 229463. https://doi.org/10.1016/j.jpowsour.2021.229463

6. Ma, R., He, J., & Deng, Y. (2022). Investigation and comparison of the electrochemical impedance spectroscopy and internal resistance indicators for early-stage internal short circuit detection through battery aging. Journal of Energy Storage, 54, 105346. https://doi.org/10.1016/j.est.2022.105346

7. Moškon, J., & Gaberšček, M. (2021). Transmission line models for evaluation of impedance response of insertion battery electrodes and cells. Journal of Power Sources Advances, 7, 100047. https://doi.org/10.1016/j.powera.2021.100047

8. Raijmakers, L. H. J., Danilov, D. L., van Lammeren, J. P. M., Lammers, M. J. G., & Notten, P. H. L. (2014). Sensorless battery temperature measurements based on electrochemical impedance spectroscopy. Journal of Power Sources, 247, 539–544. https://doi.org/10.1016/j.jpowsour.2013.09.005

9. Schindler, S., & Danzer, M. A. (2017). Influence of cell design on impedance characteristics of cylindrical lithium-ion cells: A model-based assessment from electrode to cell level. Journal of Energy Storage, 12, 157–166. https://doi.org/10.1016/j.est.2017.05.002

10. Son, Y., Cha, H., Lee, T., Kim, Y., Boies, A., Cho, J., & De Volder, M. (2024). Analysis of differences in electrochemical performance between coin and pouch cells for lithium-ion battery applications. Energy & Environmental Materials, 7, e12615. https://doi.org/10.1002/eem2.12615

11. Ulrich, J., Lindner, A., Brake, T., Winter, M., Wiemers-Meyer, S., Weber, A., & Krewer, U. (2025). Early detection of lithium plating during fast charging of lithium-ion batteries using nonlinear frequency response analysis. Journal of Power Sources, 647, 237358. https://doi.org/10.1016/j.jpowsour.2025.237358

12. Wang, L., Song, Z., Zhu, L., & Jiang, J. (2023). Fast electrochemical impedance spectroscopy of lithium-ion batteries based on the large square wave excitation signal. iScience, 26(4), 106463. https://doi.org/10.1016/j.isci.2023.106463

13. X.-Y. Yao, S. Saxena, L. Su, & Pecht, M. G. (2019). The explosive nature of tab burrs in Li-ion batteries. IEEE Access, 7, 45978–45982. https://doi.org/10.1109/ACCESS.2019.2909018

14. Yue, Z., Dunya, H., Ashuri, M., Kucuk, K., Aryal, S., Antonov, S., Alabbad, B., Segre, C. U., & Mandal, B. K. (2020). Synthesis of a very high specific surface area active carbon and its electrical double-layer capacitor properties in organic electrolytes. ChemEngineering, 4(3), 43. https://doi.org/10.3390/chemengineering4030043

Document Number: ELECTIMPSPECWP REV 0